saline starting on the day of surgery (RK; n=21) and the B) renal ablation group treated with 1 mg/kg/day telmisartan, starting on the day of surgery (RK-ARB; n=21). Seven rats from each of the two groups were examined 2, 4, and 8 weeks after the operation. The minipumps were exchanged every 4 weeks. After observation, the right kidney was removed and processed, as described in the Animal models. This was considered the control kidney. All the rats were maintained under similar housing/feeding conditions as the sham rats. The sham rats were not treated with telmisartan during the research period.

Blood urea nitrogen levels and creatinine clearance in blood and urine

Renal function was evaluated by blood urea nitrogen (BUN) levels and creatinine clearance (Ccr). Blood samples were obtained from the tail vein before the operation and at the end of treatment. Serum was obtained by centrifuging blood samples at 3,000 rpm for 20 minutes at 4°C. For urine samples, the rats were placed in individual cages for 24 hours. After the urine volume was measured, samples were collected and centrifuged at 3,000 rpm for 10 minutes at 4°C. The supernatants were used for the creatinine concentration assay. Blood and urine samples were stored at −20°C until the assay. Each Ccr value was measured using enzyme-linked immunoassay kits (Cayman Chemical Company, Ann Arbor, MI, USA). The BUN was measured using the Wako BUN-test (Wako Pure Chemical Industries, Ltd, Osaka, Japan); the absorbance was detected at 570 nm for BUN and at 492 nm for creatinine, using a microplate reader (Thermo/LabSystems Multiskan RC, Artisan Technology Group®, Champaign, IL, USA).

Measurement of Hyp

Hyp was evaluated according to previous reports.[14,15] The tissue homogenate was hydrolyzed in alkali. The hydrolyzed sample was mixed with a buffered chloramine-T reagent, and oxidation was allowed to proceed for 25 minutes at room temperature. The chromophore was developed with the addition of an Ehrlich's reagent. The absorbance was read at 550 nm using an absorption spectrophotometer (Thermo/LabSystems Multiskan RC).

Histological assessment

At 2, 4, and 8 weeks after the left nephrectomy or sham operation, the rats were sacrificed. The remnant kidneys were removed, fixed in 10% buffered formalin, and embedded in paraffin. Subsequently, 4 μm-thick sections were stained with hematoxylin and eosin (H&E) stain and Masson's trichrome (MT) stain for light microscopy. Quantitative data for percentage of fibrotic area were measured in three to six different fields per MT-stained specimen. Slides were evaluated twice at different times by two investigators (TM and YS).

RNA extraction and quantitative analysis of AT1R using RT-PCR

The expression of AT1R mRNA in the renal cortex was assessed by RT–PCR, as described previously.[16] The kidney was preserved with RNA*later*™ (Ambion, Inc, Austin, TX, USA) for RT–PCR and frozen at −80°C. Frozen renal cortex (20–30 mg) was homogenized in 1 mL of QIAzol reagent (QIAGEN Inc, Valencia, CA, USA) using a polytron homogenizer for 30 seconds. For RT–PCR, RNA was extracted from the kidney cortex using an RNeasy Mini Kit (QIAGEN), and it was stored at −80°C. The AT1R gene expression was analyzed by real-time quantitative RT–PCR performed using the TaqMan system on the basis of real-time detection of accumulated fluorescence (ABI Prism 7700; PerkinElmer, Waltham, MA, USA).[17] Prevalidated primers and probes for the AT1a receptor (Rn00578456_m1) were obtained via Assays-on-Demand (Applied Biosystems, product line of Life Technologies, Carlsbad, CA, USA). Total RNA yields were determined by spectrophotometry. The amplification was performed using the method of Cao et al.[18]

Protein extraction and Western blotting for AT1R and TGF-β

Protein levels of the AT1R in the renal tissues were analyzed by Western blotting, as previously described.[15,19,20] The membrane was reacted with a polyclonal anti-AT1 receptor antibody (1:1,000; Santa Cruz Biotechnology Inc, Santa Cruz, CA, USA), followed by incubation with a horseradish peroxidase-conjugated secondary antibody (for the AT1 receptor: goat antirabbit IgG, 1:1,000; Santa Cruz Biotechnology Inc, Santa Cruz, CA, USA). To check for equal loading, membranes were reprobed with an antibody against β-actin (Sigma Chemicals, Perth, WA, Australia).

Statistical analysis

Results were expressed as mean ± standard error of mean. Statistical comparisons were made by analysis of variance, followed by the Kruskal–Wallis test. All statistical analyses were two-sided, and significance was defined as a P value of <0.05. All statistical analyses were performed on a personal computer with the statistical package StatView

for Windows (version 5.0, Abacus Concept, Inc, Berkeley, CA, USA).

Results

Changes of renal function and fibrosis

We compared kidney weight (KW), body weight (BW), and its ratio (KW/BW) in all groups. At baseline, there was no significant difference in any parameters among the groups. At 2 weeks, the KW/BW of the RK (3.89 ± 0.40) and the RK-ARB (3.76 ± 0.23) groups was significantly higher than that of the Sham group (3.37 ± 0.18, $P<0.01$). However, there was no significant difference between the two nephrectomized groups ($P=0.07$). At 8 weeks, although KW/BW in the RK-ARB group (3.99 ± 0.27) tended to be lower than that in the RK group (4.16 ± 0.26), this difference was not significant ($P=0.10$). Finally, there was no significant difference in BW and KW between these two groups at any time point.

Changes in the BUN levels are shown in Figure 1A. At 2 weeks, significant increases of the BUN levels compared with the baseline were observed in both the RK and the RK-ARB groups. On the other hand, no significant differences were noted at the other time points in either the RK or the RK-ARB groups.

Next, we examined changes in Ccr (Figure 1B). Ccr in the RK group decreased significantly after 2 weeks when compared with that in the Sham group ($P<0.01$) and, after 4 weeks, compared with that in the RK-ARB group ($P<0.01$). However, although Ccr in the RK-ARB group had a trend to be lower than in the Sham group at 2 and 4 weeks, the differences were not significant ($P=0.73$ and $P=0.23$, respectively).

Changes in the Hyp levels are shown in Figure 1C. Progressive increases in the Hyp levels were detected in the RK group. Such increases were significant when compared with the baseline after 2 weeks. In addition, the Hyp levels in the RK group were significantly higher ($P<0.01$) than those at the corresponding time point in the RK-ARB group from 4 weeks after nephrectomy (Figure 1C).

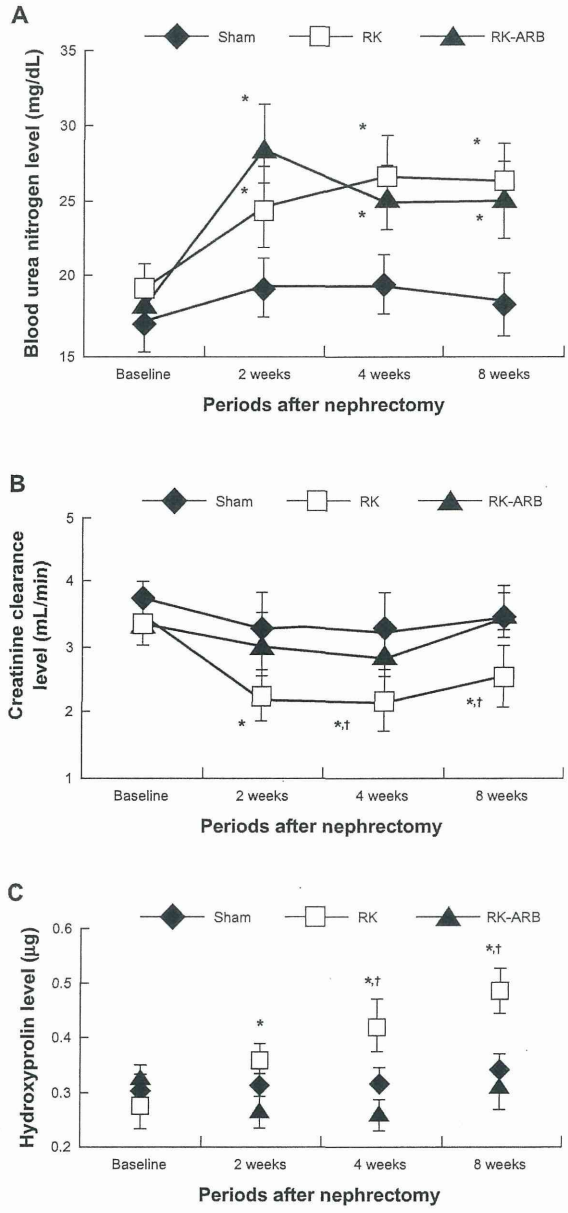

Figure 1 Course of changes in BUN, Ccr, and Hyp levels in the three rat groups.
Notes: Figure 1(**A–C**) showed the time course of changes in BUN, Ccr, and Hyp levels in the three rat groups. *$P<0.05$ versus Sham group rats at the same time. †$P<0.05$ versus RK-ARB at the same time.
Abbreviations: RK, rat-remnant kidney; ARB, angiotensin II type I receptor blocker; BUN, blood urea nitrogen; Ccr, creatinine clearance; Hyp, hydroxyproline; Sham, sham-operated group.

Histopathological changes

Figure 2A–C show H&E-stained samples. However, there was no significant change in the renal tissue in any of the three rat models. The representative examples of MT staining and the percentage of fibrotic area in rat tissues are shown in Figure 2D–J, respectively. At first, we examined control kidney tissues at the baseline (Figure 2D) and at 8 weeks (Figure 2E). We noticed no differences between the control tissues in any specimens. Figure 2F and G are representative examples of MT-stained sections in the RK group at 2 and 8 weeks, respectively. The fibrous area in the RK group at 2 weeks (20.8% ± 4.9%, Figure 2F) was larger ($P<0.01$) than that in the Sham group, including those at 8 weeks (10.8% ± 2.0%, Figure 2D). In addition, fibrosis in the RK group at 8 weeks (53.3% ± 5.2%, Figure 2G)

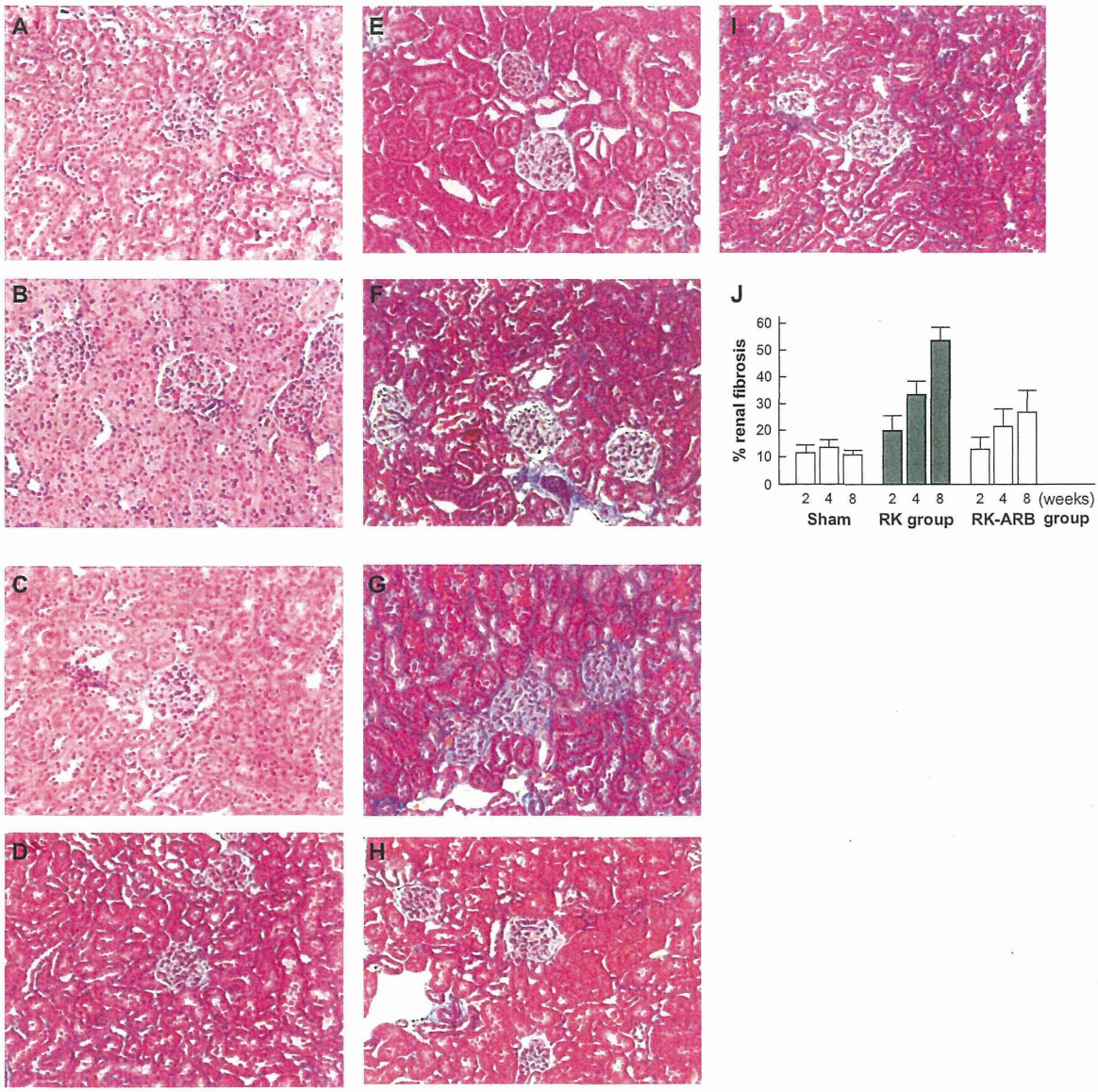

Figure 2 (**A**–**C**) show a section stained with H&E staining.
Notes: There were no changes in the glomeruli or renal tubules in any of the three rat groups after 8 weeks – (**A**) Sham group; (**B**) RK group; and (**C**) RK-ARB group. Figure 2 (**D**–**I**) show representative examples of MT staining. Control kidney tissues at baseline and at 8 weeks are shown in Figure 2**D** and **E**, respectively. Fibrosis in the RK group at 2 weeks (Figure 2**F**) was significantly different ($P<0.01$), compared with that in the RK groups at 8 weeks (Figure 2**G**). Figure 2**H** and **I** show representative specimens in the RK-ARB at 2 weeks and at 8 weeks, respectively. (Original magnification, ×200). The percentage of fibrous area in the RK-ARB group was significantly lower ($P<0.01$) than that in the RK group at each week (Figure 2**J**).
Abbreviations: RK, rat-remnant kidney; ARB, angiotensin II type I receptor blocker; MT, Masson's trichrome; H&E, hematoxylin and eosin; sham, sham-operated group.

was significantly different ($P<0.01$) compared with that in the Sham and the RK groups at 2 weeks (Figure 2F). In particular, marked sclerosis of the glomeruli was observed in the RK group at 8 weeks (Figure 2G). Thus, the fibrotic area increased considerably with time after nephrectomy in the RK group. Although a similar trend was also seen in the RK-ARB group at 2 weeks (Figure 2H) and at 8 weeks (Figure 2I), the percentage of fibrous area in the RK-ARB group was significantly lower than that in the RK group at each week (Figure 2J).

Altered mRNA and protein levels of AT1R

Changes in the mRNA expression of AT1R are shown in Figure 3. In the RK group, AT1R was upregulated immediately compared with the RK-ARB group. At 2 weeks, the

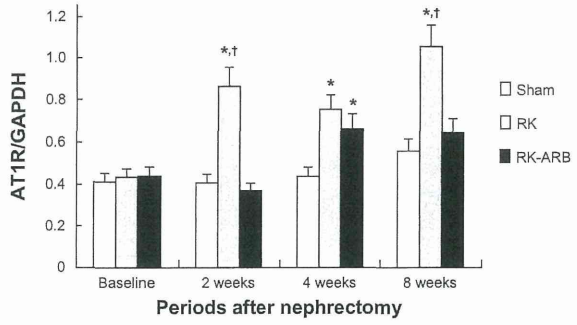

Figure 3 Altered AT1R mRNA expression levels.
Notes: Significant increases in the AT1R mRNA expression were observed 2 weeks after the first operation in the RK group. Although AT1R mRNA expression level in the RK-ARB group was higher than that in the Sham group at 4 weeks, the expression was suppressed in the RK-ARB group at 8 weeks, and no significant difference was found between the Sham and RK-ARB groups at 8 weeks. *$P<0.05$ versus the Sham group. †$P<0.05$ versus the RK-ARB group.
Abbreviations: AT1R, angiotensin II type I receptor; GAPDH, glyceraldehyde 3-phosphate dehydrogenase; RK, rat-remnant kidney; ARB, angiotensin II type I receptor blocker; sham, sham-operated group.

AT1R mRNA expression in the RK group was significantly higher ($P<0.01$) than that in the Sham and the RK-ARB groups (Figure 3). In addition, such increases compared with the Sham group were noted for all time points. On the other hand, in the RK-ARB group, mRNA expression showed significant differences compared with the Sham group at 4 weeks ($P<0.01$). However, unlike the RK group, significant differences between the RK-ARB and Sham groups were not detected at 8 weeks.

Representative examples of the Western blotting regarding AT1R expression are shown in Figure 4A. Increased AT1R expression compared with the Sham group was found at all time points for the RK group, and the AT1R expression levels increased with time. On the other hand, such expression was not found in the RK-ARB group at any time point.

Altered protein levels of TGF-β

The TGF-β expression is shown in Figure 4B. In the RK group, increases in the TGF-β expression were noted from 2 weeks after surgery. However, increasing TGF-β expression with time was not found in the RK group. On the other hand, in the RK-ARB group, low TGF-β expression was found at all time points, and all of the TGF-β expression levels were similar. When the correlation between the AT1R expression and the TGF-β expression was analyzed using relative densitometric levels of each protein per unit of β-actin, no significant correlation was detected. Similarly, we found no significant relationship between the AT1R gene expression and the TGF-β expression (Figures 3 and 4B).

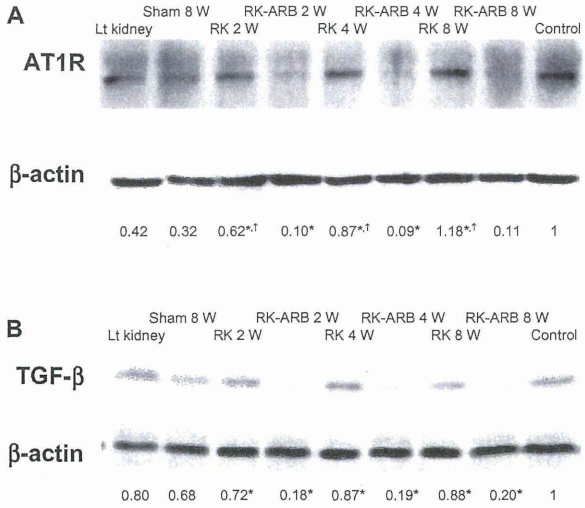

Figure 4 Altered protein levels of AT1R.
Notes: Western blotting revealed AT1R expression in the RK group was higher than in the Sham and the RK-ARB groups. Numbers represent relative densitometric levels of AT1R per unit β-actin in the pellets. *$P<0.01$ RK versus RK-ARB at 2 weeks, 4 weeks, and 8 weeks; †$P<0.05$ RK at 2 weeks versus RK at 4 weeks; RK at 2 weeks versus RK at 8 weeks; and RK at 4 weeks versus RK at 8 weeks. Figure 4B shows the altered TGF-β protein levels. In the RK group, significant increases in the TGF-β expression were observed at 2 weeks after the first operation. Numbers represent relative densitometric levels of TGF-β per unit β-actin in the pellets. *$P<0.01$ RK at 2 weeks versus RK-ARB at 2 weeks; RK at 4 weeks versus RK-ARB at 4 weeks; and RK at 8 weeks versus RK-ARB at 8 weeks.
Abbreviations: AT1R, angiotensin II type I receptor; Lt, left; RK, rat-remnant kidney; ARB, angiotensin II type I receptor blocker; TGF- β, transforming growth factor beta; w, weeks; sham, sham-operated group.

Discussion

Many investigators have reported that blockage of the RAS by ARBs could maintain renal function in various types of nephropathy.[12,13,21] In addition to examining chronic renal failure progression, a study used 5/6 nephrectomized rat models to clarify the renoprotective effects of ARBs in acute renal failure.[22] In contrast, this is the first report regarding changes of renal function and pathological features induced by ARBs under unilateral nephrectomized conditions that do not represent renal failure.

The present study detected that the use of telmisartan resulted in a decrease in AT1R mRNA and protein expression. AT1R is known to mediate most of the physiological and pathological effects of angiotensin II, such as hyperdynamic actions, endocrine functions, and mitogenic effects in the kidney.[23–26] Thus, understanding the mechanism of the AT1R expression in kidney tissues under pathological conditions is important to discuss potential strategies to maintain renal function. With regard to the relationship between the AT1R and ARBs, there is a report that the AT1R expression was suppressed by telmisartan at both the mRNA and the protein levels in vascular smooth muscle cells.[27] However, to our knowledge,

this is the first report on changes of the AT1R expression after using telmisartan in kidney tissues under pathological conditions. Our results showed that both the expression of AT1R mRNA and protein in the RK-ARB group were significantly lower than those in the RK group. On the basis of these facts, we speculate that the suppression of AT1R expression is an important mechanism underlying the renoprotective effect of telmisartan. On the other hand, telmisartan also induces peroxisome proliferator-activated receptor gamma (PPARγ). Furthermore, PPARγ is associated with fibrosis under a variety of conditions.[28] Therefore, in addition to AT1R-related activities, investigations regarding the change of PPARγ-related activation, including the regulation of fibrosis under unilateral nephrectomized conditions, are necessary.

Another interesting finding of this study was that TGF-β expression in the RK-ARB group was lower than that in the RK group. TGF-β has been shown to mediate various key renal pathological events, including fibrosis, during loss of renal function.[29] In addition, TGF-β also induces autophagy and apoptosis, leading to fibrosis, in renal tissues.[30] Thus suppression of the TGF-β expression leads to protection of renal function. We speculate that telmisartan may protect renal function via the regulation of some of these mechanisms. Our results also showed that the Hyp expression, a marker of fibrosis, was suppressed by telmisartan. Interestingly, AT1R was reported to be a regulator of TGF-β in nephropathy.[31] From these facts, we hypothesized that suppressed AT1R expression by telmisartan would lead to the inhibition of TGF-β expression in this renal dysfunction model. Unfortunately, our results did not show a significant correlation between the TGF-β expression and the AT1R expression. Thus, it is likely that the TGF-β expression in kidney tissues is regulated by other factors under pathological conditions.

Our study showed that telmisartan was effective in maintaining Ccr. On the other hand, pathological features evaluated by H&E staining showed no differences between the RK and the RK-ARB groups. The unilateral nephrectomy model is thought to result in relatively mild damage to the remnant kidney compared with the 5/6 nephrectomy model.[22] In recent years, partial nephrectomy has been recommended for patients with low-stage RCC to maintain renal function. Our results support this strategy from the renoprotective perspective.

In this study, we used telmisartan, which is structurally and functionally unique among ARBs. Although most ARBs are biphenyl–tetrazole derivatives, telmisartan is a biphenyl–nontetrazole derivative and has greater lipophilicity and a longer half-life. In addition, interestingly, the anti-inflammatory and fibrous effects of telmisartan are the result of the PPARγ activation. These characteristics favor the renoprotective effect. Several reports have shown that telmisartan has better renal protective effects than other ARBs in nephropathy.[21,32] Further studies are necessary to determine whether such findings are common with other ARBs. Detailed investigations and a good understanding of the renoprotective function of ARBs are essential for the treatment and observation of chronic kidney disease.[33]

One of the major limitations of this study is that we used only a single ARB, ie, telmisartan. Therefore, no direct comparison within this study regarding the general effects of ARBs could be made. Another limitation is the lack of data regarding blood pressure. Telmisartan suppressed blood pressure in various animal models with renal dysfunction. It is possible that this also occurred in our study. On the other hand, we have some evidence that telmisartan may cause symptomatic hypotension in patients with nephrectomy (data not shown). A further limitation is that our results showed no significant difference on renal function when evaluated by BUN levels and Ccr. In addition, we have no data regarding other functional parameters affected by fibrosis. Although we speculated that the renoprotective function of telmisartan might be undervalued in the relatively early phase after nephrectomy, this study has little evidence to confirm this. Thus, more detailed clinical studies and pathological examinations, including the renoprotective and hypotensive function of telmisartan after unilateral ablation, are necessary.

Conclusion

It can be concluded that the ARB telmisartan protected renal function after nephrectomy in a rat model. This conforms to the preexisting clinical evidence. In terms of the mechanism of the renoprotective effects, inhibition of fibrosis was important, and AT1R and TGF-β are speculated to be important in the regulation of fibrotic changes.

Acknowledgment

We are grateful to Takumi Shimogama for his support.

Disclosure

The authors report no conflicts of interest in this work. This study was not supported financially by any funding agency or company.

References

1. Martin FL, McKie PM, Cataliotti A, et al. Experimental mild renal insufficiency mediates early cardiac apoptosis, fibrosis, and diastolic dysfunction: a kidney-heart connection. *Am J Physiol Regul Integr Comp Physiol*. 2012;302(2):R292–R299.

2. Szymanski MK, Damman K, van Veldhuisen DJ, van Gilst WH, Hillege HL, de Boer RA. Prognostic value of renin and prorenin in heart failure patients with decreased kidney function. *Am Heart J*. 2011;162(3):487–493.
3. Parvanova A, Chiurchiu C, Ruggenenti P, Remuzzi G. Inhibition of the renin-angiotensin system and cardio-renal protection: focus on losartan and angiotensin receptor blockade. *Expert Opin Pharmacother*. 2005;6(11):1931–1942.
4. Shiga Microalbuminuria Reduction Trial (SMART) Group, Uzu T, Sawaguchi M, Maegawa H, Kashiwagi A. Reduction of microalbuminuria in patients with type 2 diabetes: the Shiga Microalbuminuria Reduction Trial (SMART). *Diabetes Care*. 2007;30(6):1581–1583.
5. Koike H, Sada T, Mizuno M. In vitro and in vivo pharmacology of olmesartan medoxomil, an angiotensin II type AT1 receptor antagonist. *J Hypertens Suppl*. 2001;19(1):S3–S14.
6. Lavoz C, Rodrigues-Diez R, Benito-Martin A, et al. Angiotensin II contributes to renal fibrosis independently of Notch pathway activation. *PLoS One*. 2012;7(7):e40490.
7. Kagami S, Border WA, Miller DE, Noble NA. Angiotensin II stimulates extracellular matrix protein synthesis through induction of transforming growth factor-beta expression in rat glomerular mesangial cells. *J Clin Invest*. 1994;93(6):2431–2437.
8. Remuzzi G, Perico N, Macia M, Ruggenenti P. The role of renin-angiotensin-aldosterone system in the progression of chronic kidney disease. *Kidney Int Suppl*. 2005;99:S57–S65.
9. Takeuchi Y, Yamauchi K, Nakamura J, Shigematsu S, Hashizume K. Angiotensin II regulates migration in mouse cultured mesangial cells: evidence for the presence of receptor subtype-specific regulation. *J Endocrinol*. 2006;191(2):361–367.
10. Mandarim-de-Lacerda CA, Pereira LM. Effect of telmisartan on preexistent cardiac and renal lesions in spontaneously hypertensive mature rats. *Histrol Histpathol*. 2004;19(3):727–733.
11. Banki NF, Ver A, Wagner LJ, et al. Aldosterone antagonists in monotherapy are protective against streptozotocin-induced diabetic nephropathy in rats. *PLoS One*. 2012;7(6):e39938.
12. Toba H, Tojo C, Wang J, Noda K, Kobara M, Nakata T. Telmisartan inhibits vascular dysfunction and inflammation via activation of peroxisome proliferator-activated receptor-γin subtotal nephrectomized rat. *Eur J Pharmacol*. 2012;685(1–3):91–98.
13. Fujimoto S, Satoh M, Horike H, et al. Olmesartan ameliorates progressive glomerular injury in subtotal nephrectomized rats through suppression of superoxide production. *Hypertens Res*. 2008;31(2):305–313.
14. Varghese Z, Moorhead JF, Wills MR. Plasma hydroxyproline fractions in patients with dialysis osteodystrophy. *Clin Chim Acta*. 1981;110(1):105–111.
15. Reddy GK, Enwemeka CS. A simplified method for the analysis of hydroxyproline in biological tissues. *Clin Biochem*. 1996;29(3):225–229.
16. Rodrigo MC, Martin DS, Redetzke RA, Eyster KM. A method for the extraction of high quality RNA and protein from single small samples of arteries and veins preserved in RNAlater. *J Pharmacol Toxicol Methods*. 2002;47(2):87–92.
17. Bonnet F, Cooper ME, Carey RM, Casley D, Cao Z. Vascular expression of angiotensin type 2 receptor in the adult rat: Influence of angiotensin II infusion. *J Hypertens*. 2001;19(6):1075–1081.
18. Cao Z, Bonnet F, Candido R, et al. Angiotensin type 2 receptor antagonism confers renal protection in a rat model of progressive renal injury. *J Am Soc Nephrol*. 2002;13(7):1773–1787.
19. Yao L, Kobori H, Rahman M, et al. Olmesartan improves endothelin-induced hypertension and oxidative stress in rats. *Hypertens Res*. 2004;27(7):493–500.
20. Nishiyama A, Yoshizumi M, Rahman M, et al. Effects of AT1 receptor blockade on renal injury and mitogen-activated protein activity in Dahl salt-sensitive rats. *Kidney Int*. 2004;65(3):972–981.
21. Bakris G, Burgess E, Weir M, Davidai G, Koval S; AMADEO Study Investigators. Telmisartan is more effective than losartan in reducing proteinuria in patients with diabetic nephropathy. *Kidney Int*. 2008;74(3):364–369.
22. Nagai Y, Yao, L, Kobori H, et al. Temporary angiotensin II blockade at the prediabetic stage attenuates the development of renal injury in type 2 diabetic rats. *J Am Soc Nephrol*. 2005;16(3):703–711.
23. Goodfriend TL, Elliott ME, Catt KJ. Angiotensin receptors and their antagonists. *N Engl J Med*. 1996;334(25):1649–1654.
24. Unger T, Culman J, Gohlke P. Angiotensin II receptor blockade and end-organ protection: pharmacological rationale and evidence. *J Hypertens Suppl*. 1998;16(7):S3–S9.
25. Duncan JA, Scholey JW, Miller JA. Angiotensin II type 1 receptor gene polymorphisms in humans: physiology and pathophysiology of the genotypes. *Curr Opin Nephrol Hypertens*. 2001;10(1):111–116.
26. Siragy HM, Carey RM. Angiotensin type 2 receptors: potential importance in the regulation of blood pressure. *Curr Opin Nephrol Hypertens*. 2001;10(1):99–103.
27. Imayama I, Ichiki T, Inanaga K, et al. Telmisartan downregulates angiotensin II type 1 receptor through activation of peroxisome proliferator-activated receptor gamma. *Cardiovasc Res*. 2006;72(1):184–190.
28. Attia YM, Elalkamy EF, Hammam OA, Mahmoud SS, El-Khatib AS. Telmisartan, an AT1 receptor blocker and a PPAR gamma activator, alleviates liver fibrosis induced experimentally by Schistosoma mansoni infection. *Parasit Vectors*. 2013;6:199.
29. López-Hernández FJ, López-Novoa JM. Role of TGF-β in chronic kidney disease: an integration of tubular, glomerular and vascular effects. *Cell Tissue Res*. 2012;347(1):141–154.
30. Xu Y, Yang S, Huang J, Ruan S, Zheng Z, Lin J. Tgf-β1 induces autophagy and promotes apoptosis in renal tubular epithelial cells. *Int J Mol Med*. 2012;29(5):781–790.
31. Koshizaka M, Takemoto M, Sato S, et al. An angiotensin II type 1 receptor blocker prevents renal injury via inhibition of the Notch pathway in Ins2 Akita diabetic mice. *Exp Diabetes Res*. 2012;2012:159874.
32. Khan AH, Imig JD. Telmisartan provides better renal protection than valsartan in a rat model of metabolic syndrome. *Am J Hypertens*. 2011;24(7):816–821.
33. Morosetti M, Gorini A, Costanzo AM. Clinical management of nondialysis patients with chronic kidney disease: a retrospective observational study. Data from the SONDA study (Survey Of Non-Dialysis outpAtients). *Int J Nephrol Renovasc Dis*. 2013;6:27–37.

Biochimica et Biophysica Acta 1830 (2013) 2204–2213

Contents lists available at SciVerse ScienceDirect

Biochimica et Biophysica Acta

journal homepage: www.elsevier.com/locate/bbagen

CHK1 cleavage in programmed cell death is intricately regulated by both caspase and non-caspase family proteases

Naoyuki Okita [a,*], Miyuki Yoshimura [b], Kazuhito Watanabe [a], Shota Minato [a], Yuki Kudo [b], Yoshikazu Higami [a], Sei-ichi Tanuma [b]

[a] Department of Molecular Pathology and Metabolic Disease, Tokyo University of Science, 2641 Yamazaki, Noda-shi, Chiba 278-0022, Japan
[b] Department of Biochemistry, Faculty of Pharmaceutical Sciences, Tokyo University of Science, 2641 Yamazaki, Noda-shi, Chiba 278-0022, Japan

ARTICLE INFO

Article history:
Received 10 April 2012
Received in revised form 18 September 2012
Accepted 10 October 2012
Available online 16 October 2012

Keywords:
CHK1
DNA damage response
Programmed cell death
Caspase family proteases
Non-caspase family proteases

ABSTRACT

Background: CHK1 is an important effector kinase that regulates the cell cycle checkpoint. Previously, we showed that CHK1 is cleaved in a caspase (CASP)-dependent manner during DNA damage-induced programmed cell death (PCD) and have examined its physiological roles.
Methods and results: In this study, we investigated the behavior of CHK1 in PCD. Firstly, we found that CHK1 is cleaved at three sites in PCD, and all cleavages were inhibited by the co-treatment of a pan-CASP inhibitor or serine protease inhibitors. We also showed that CHK1 is cleaved by CASP3 and/or CASP7 recognizing at ^{296}SNLD^{299} and ^{348}TCPD^{351}, and that the cleavage results in the enhancement of CHK1 kinase activity. Furthermore, as a result of the characterization of cleavage sites by site-directed mutagenesis and an analysis performed using deletion mutants, we identified ^{320}EPRT^{323} as an additional cleavage recognition sequence. Considering the consensus sequence cleaved by CASP, it is likely that CHK1 is cleaved by non-CASP family protease(s) recognizing at ^{320}EPRT^{323}. Additionally, the cleavage catalyzed by the ^{320}EPRT^{323} protease(s) markedly and specifically increased when U2OS cells synchronized into G1 phase were induced to PCD by cisplatin treatment.
Conclusion: CHK1 cleavage is directly and indirectly regulated by CASP and non-CASP family proteases including serine protease(s) and the "^{320}EPRT^{323} protease(s)." Furthermore, ^{320}EPRT^{323} cleavage of CHK1 occurs efficiently in PCD which is induced at the G1 phase by DNA damage.
General significance: CASP and non-CASP family proteases intricately regulate cleavage for up-regulation of CHK1 kinase activity during PCD.

1. Introduction

DNA damage induced by anti-cancer drugs, ultraviolet light and ionizing radiation compromises the maintenance of genomic integrity. Cells of multicellular organisms harbor two major pathways to protect from DNA damage. DNA repair initiated at the cell cycle checkpoint is the initially responsive protective machinery and contributes to cell survival. Programmed cell death (PCD) provides a further response to protect against DNA damage. Failure of these mechanisms threatens the survival of individual organisms via aberrant cell survival and cancer progression. One of the signature apoptotic mechanisms is cleavage of various cellular proteins by the caspase (CASP) family [1,2]. Within the CASP family, CASP2, CASP3, CASP6, CASP7, CASP8, CASP9, and CASP10 are categorized as apoptotic CASPs, which orchestrate the apoptotic cascade [1–5]. Although all CASPs including inflammatory CASPs display preferential recognition, it is required that the P1 residue, which is the site of cleavage, is an aspartic acid [3–5]. The involvements of non-CASP family proteases including certain serine proteases, calpains and lysosomal proteases in various modes of PCD including apoptotic cell death have also been reported [6]. These findings have suggested that apoptotic protease is not only CASP family protease. However, it remains unclear whether these non-CASP family proteases regulate apoptotic cell death directly or indirectly (for example, via other modes of PCD). Taken together, protein cleavage by proteases may be a common regulatory mechanism of various modes of PCD.

Regulatory factors in DNA damage response such as PARP1, RAD51, ATM, RAD9, CLASPIN, CHK1, and MDC1 have been reported as "death substrates" cleaved by apoptotic CASPs in PCD [7–13]. On the other hand, it has been less reported about cleavage of proteins involved in DNA damage by non-CASP family proteases. Since DNA damage response consists of various physiological processes (for example, DNA damage recognition, DNA repair, and cell cycle checkpoint etc.), it is important to understand the mechanisms and roles of the cleaved proteins in PCD regulation. Furthermore, one unresolved question in DNA damage-induced PCD concerns whether the PCD

* Corresponding author at: Department of Molecular Pathology and Metabolism, Faculty of Pharmaceutical Sciences, Tokyo University of Science, 2641 Yamazaki, Noda-shi, Chiba 278-0022, Japan. Tel./fax: +81 4 7121 3676.
E-mail addresses: nokita7@rs.noda.tus.ac.jp, nmsokita@gmail.com (N. Okita).

0304-4165/$ – see front matter © 2012 Elsevier B.V. All rights reserved.
http://dx.doi.org/10.1016/j.bbagen.2012.10.009

regulation at each cell cycle phase is identical. For example, mitotic catastrophe is one of the PCD pathways induced at M phase [1,2]. While CASP activation is observed during mitotic catastrophe, the regulation mechanism is not always identical to apoptotic cell death [1,2]. Furthermore it was shown that mitotic catastrophe executes in cell death by CASP-dependent and -independent mechanisms [14]. While scientific evidence with regard to cell cycle-specific PCD has been little shown, these findings with regard to mitotic catastrophe suggests the existence of cell cycle-selective PCD pathways.

We have previously investigated the mechanism of DNA damage-induced PCD and discovered that CHK1, an important effector kinase that regulates the cell cycle checkpoint, is cleaved in a CASP-dependent manner during etoposide-induced PCD [12]. Another group subsequently demonstrated that the CASP cleavage sites of CHK1 are D^{299} and D^{351} [15]. Furthermore, it was recently reported that the CHK1 signaling pathway controls PCD [16,17]. These findings indicate that CHK1 may be one of the key molecules that link the checkpoint to PCD. In this study, we focus on the behavior of CHK1 in DNA damage-induced PCD and demonstrate the involvements of CASP and non-CASP family proteases in CHK1 cleavage. Our results suggest that CHK1 cleavage is intricately regulated during DNA damage-induced PCD and provide a good model of dual regulation by CASP and non-CASP family proteases.

2. Materials and methods

2.1. Cells and drugs

U2OS and HeLaS3 cells were maintained in DMEM (WAKO, Osaka, Japan) supplemented with 10% fetal calf serum (BOVOGEN, East Keilor, VIC, Australia) and 1% penicillin/streptomycin (SIGMA, St. Louis, MO, USA). For immunocytochemistry, cells were seeded on poly-D-lysine-coated glass coverslips and subsequently treated. Anti-Fas (clone CH11) was supplied by MBL (Aichi, Japan). Benzyloxycarbonyl-Val-Ala-Asp (OMe) fluoromethylketone (z-VAD-fmk) and *N*-carbobenzoxyl-L-leucinyl-L-leucinyl-L-norvalinal (LLnV) were from Peptide Institute (Osaka, Japan). *N*-Acetyl-L-leucyl-L-leucyl-L-norleucinal (LLnL) was purchased from Merck (Darmstadt, Germany). All other drugs were purchased from WAKO.

2.2. Western blotting

Cells were lyzed by the addition of lysis buffer (50 mM Tris–HCl pH 6.8, 2% SDS, 5% glycerol), boiled for 5 min, and sonicated. Protein concentrations of the soluble fraction were determined by the BCA protein assay (Thermo Fisher Scientific, Rockford, IL, USA) according to the manufacturer's protocol, and standardized by the addition of lysis buffer. 2-ME (5%) and bromophenol blue (0.025%) were subsequently added to protein solutions and the mixtures were boiled for 5 min. Equal amounts of proteins (5–20 μg) were subjected to SDS-PAGE and transferred to nitrocellulose membranes. The membranes were blocked with 2.5% skim milk and 0.25% BSA in TBS (50 mM Tris, pH 7.4, 150 mM NaCl) containing 0.1% Tween 20 (TTBS) for 1 h at room temperature, and probed with the appropriate primary antibodies overnight at 4 °C or for 2 h at room temperature. After washes with TTBS, the membranes were incubated with the appropriate secondary antibody, horseradish peroxidase-conjugated F(ab′)2 fragment of goat anti-mouse IgG, anti-rabbit IgG, or anti-rat IgG (Jackson Immunoresearch Laboratories, West Grove, PA, USA), for 1 h at room temperature. After washing the membrane with TTBS, the membranes were incubated with ImmunoStar LD reagent (WAKO). The specific proteins were visualized with LAS3000 (FUJI FILM, Tokyo, Japan), and the data were analyzed using MultiGauge software (FUJI FILM).

2.3. Antibodies

As primary antibodies, anti-β-actin (clone AC-15, SIGMA, USA), anti-CASP-3 (clone 1F3, MBL, Japan), anti-CASP-7 (Cell Signaling Technology, USA), anti-CASP-9 (Cell Signaling Technology, USA), anti-CHK1 N-ter (clone DCS-310, MBL, Japan), anti-CHK1 C-ter (clone EP691Y, Epitomics, USA), anti-Cyclin D1 (clone DCS-6, MBL, Japan), anti-HTRA2 (clone 18-1-83, MBL, Japan), anti-MPM2 (clone MPM-2, Millipore, USA), anti-Myc (clone PL14, MBL, Japan), and anti-Parp1 (clone C-2-10, WAKO, Japan) antibodies were used.

2.4. Site-directed mutagenesis

Site-directed mutagenesis was performed by an overlap extension method using pcDNA-FLAG-CHK1wtsm-MycHis as a template DNA. Overlap extension reaction (15 μL) was performed using 1.5 unit Accuprime Pfx polymerase (Invitrogen), 200 ng template DNA, and 4.5 pmol each forward and reverse primers under the following conditions: initiation step, 94 °C for 3 min; cycling steps, 25 cycles of at 94 °C for 1 min, at 55 °C for 30 s, at 68 °C for 4.5 min; termination step, at 68 °C for 4.5 min. After incubation at 98 °C for 1 min, the reaction product was slowly cooled down to room temperature. For digestion of template DNA, the reaction product was treated with 20 unit Dpn I (New England Biolabs, UK) at 37 °C for 2 h and was directly used for transformation.

2.5. Construction of various CHK1 vectors

For CHK1 cleavage mutant vectors, CHK1 mutant cDNA digested from the pcDNA-FLAG-hCHK1 mutant sm-MycHis by *Hin*dIII and *Pme*I was cloned into the same sites of pIRES2-EGFP. For tetracycline-inducible recombinant CHK1 expression vectors, CHK1sm cDNA was amplified by PCR using Kozak-3FLAG-CHK1-F and 3Myc CHK1-R primers. After phosphorylation of the 5′ ends by T4 polynucleotide kinase (TaKaRa), the cDNA fragment was cloned into EcoRV-digested pTRE2-hyg. For CHK1 deletion mutant expression vectors, cDNAs of C- or N-terminal deletion CHK1 mutant containing 3× Myc tag were constructed via two steps of PCR. In the first step, a DNA fragment coding a deletion mutant was amplified by PCR using phCHK1smD299E-IRES2-EGFP or phCHK1smD351E-IRES2-EGFP (as a DNA template), a forward primer for deletion mutant, and a reverse primer (kozak-CHK1-F for C-terminal deletion or CHK1-R for N-terminal deletion). In the second step, a deletion mutant cDNA fragment containing 3× Myc tag sequence was amplified by PCR using a DNA fragment amplified in the first step (as a DNA template) and a primer set (kozak-CHK1-F and 3Myc-R for C-terminal deletion or kozak-ATG-3Myc-F and CHK1-R for N-terminal deletion). After phosphorylation of the 5′ ends by T4 polynucleotide kinase, the cDNA fragment was cloned into *Sma*I-digested pIRES2-EGFP. The primer sequences for deletion mutants or point mutants used were listed in Supplemental Table SI or SII, respectively.

2.6. Preparation of recombinant CHK1

U2OS tet-on cells (Clontech, Japan) were transfected with *Nru*I-linearized pTRE2-hyg vectors containing 3× FLAG-CHK1(WT)–3× Myc, 3× FLAG-CHK1(D299E)–3× Myc, or 3× FLAG-CHK1(D351E)–3× Myc cDNA using Fugene HD (Promega, USA) according to the manufacture's protocol. Each stable transfectant was selected with 600 μg/mL hygromycin B. Established U2OS tet-on/Chk1 cells were maintained in DMEM containing 10% FCS, 1% penicillin-streptomycin solution, 120 μg/mL hygromaycin B, and 200 μg/mL G418. For induction of recombinant CHK1s, U2OS tet-on/Chk1 cells were grown in the presence of 5 μg/mL of doxycycline for 2 days. The recombinant CHK1s were purified with anti-FLAG beads (SIGMA) and anti-Myc beads (MBL).

2.7. Production of recombinant CASPs

6× His-tagged active CASPs were prepared with recombinant protein expression methods using pET system, with minor modifications, as described in elsewhere [4]. CASP2 and the other CASPs were fused 6× *His tag at the N-terminus and the C-terminus*, respectively. The expressed active CASPs were purified with TALON resin (Clontech).

2.8. CASP cleavage assay

Recombinant active CASP2, CASP3, CASP6, CASP7, CASP8, CASP9, and CASP10 were obtained as described in the supplemental information. Recombinant CHK1 was incubated with each recombinant CASP in CASP assay buffer (20 mM HEPES–NaOH, pH 7.4, 15 mM $MgCl_2$, 0.01% Nonidet-P40, 5% glycerol, 10 mM DTT) at 37 °C for 8 or 24 h. For Western blotting analysis of cleavage profile, the reaction was stopped by the addition of SDS sample buffer. For kinase activity analysis, aliquots of reaction mixture were subjected to CHK1 kinase assays.

2.9. CHK1 kinase assay

Recombinant GST-CDC25C fragment was expressed and purified as described elsewhere [18]. Recombinant CHK1 was incubated with GST-CDC25C fragments at 37 °C for 30 min, and the reaction was stopped by the addition of SDS sample buffer. The kinase activity was visualized using Western blotting and quantified by chemiluminescense.

2.10. Cell synchronization and flow cytometry

For cell cycle synchronization, double thymidine block (DTB) or thymidine nocodazole block (TNB) methods were performed. For DTB, U2OS cells were seeded at 1.6×10^4 cells/cm^2. The next day, for the first synchronization, cells were treated with 2 mM thymidine for 21 h. For second synchronization, cells were incubated for a further 12 h in growth medium without thymidine, and treated with 2 mM thymidine and 12.5 μM deoxycytidine for 15 h. The G1/S synchronized cells were then released into growth medium. S or G2 phase-enriched cells were obtained at 4.5 or 8 h from release, respectively. For G1 phase-enriched cells, M phase cells obtained by release for 11 h followed by shake-off method were cultured in growth medium for 6 h. For TNB, U2OS cells were seeded at 1.6×10^4 cells/cm^2. The next day, for first synchronization, cells were treated with 2 mM thymidine for 21 h. After incubation for 6 h in growth medium without thymidine, for second synchronization the cells were treated with 200 nM nocodazole for 6 h. The mitosis-arrested cells obtained by the shake-off method were re-seeded at 1 to 2×10^4 cells/cm^2 for G1- or S-phase synchronization. G1 or S phase-enriched cells were obtained at 6 or 12 h from release, respectively. The cell cycle distribution was confirmed by flow cytometric analysis using propidium iodide (PI) staining as described below. Harvested cells were suspended in PBS and fixed with 70% ethanol at −20 °C overnight. The fixed cells were treated with 50 μg/mL PI and 200 μg/mL RNaseA at RT for 30 min, and were then analyzed by a FACS LSR flow cytometer (BD Biosciences, San Jose, CA, USA). Cell cycle data analysis was performed with CellQuest software (BD Biosciences).

2.11. RNAi

RNAi was performed using lipofectamine RNAiMAX reagent (Invitrogen, Carlsberg, CA, USA) according to the manufacture's protocol. Stealth siRNAs were purchased from Invitrogen. The target sequences were as follows: CASP3, ATAGAACCACTATGAAGCTACCTCA: CASP7, GGGTGAATGACAGAGTTGCCAGGCA: HTRA2, GGGAGGTGATTGGAGTG AACACCAT: Scramble (eGFP), CCAACUUGUCUGGUGUCAAAAAUAA.

3. Results

3.1. CHK1 cleavage in PCD and the involvement of CASP and serine protease families.

We previously demonstrated that CHK1 is cleaved during DNA damage-induced PCD in HeLa S3 cells [12]. This phenomenon appeared to be regulated by a CASP-dependent pathway, because a pan-caspase inhibitor, z-VAD-fmk, abolished CHK1 cleavage during DNA damage-induced PCD. In this study, we sought to perform further analysis of CHK1 cleavage during PCD. We treated U2OS cells with either etoposide (Etp) or cisplatin (Cis), at two different dosage levels, to induce moderate (cell viable) or severe (cell nonviable) DNA damage. The moderate and severe doses both induced DNA damage responses such as with CHK1 and H2AX phosphorylation (data not shown) in a dose-dependent manner. In cell lysates treated with higher doses, we detected several cleavage products with lower molecular weights than that of full-length CHK1. Interestingly, CHK1 was efficiently cleaved during DNA damage-induced PCD such as with Cis, camptothecin (Cpt) and Etp (Fig. 1B). The molecular weights of the products recognized by anti-CHK1 C-ter were approximately 15, 17 and 20 kDa (termed C1, C2, and C3, respectively) and those of products recognized by anti-CHK1 N-ter were approximately 42, 40 and 37 kDa (termed N1, N2, and N3). Considering that the molecular weight of full-length CHK1 is approximately 57 kDa, it is likely that N3–C3 and N1–C1 are cleavage products at D^{299} and D^{351}, respectively [15], and N2–C2 are from the unknown recognition sequence that is located between D^{299} and D^{351}. Our estimation of this combination was also supported by the product composition: in Cis treatment, C3 = C2 > C1 and N3 = N2 > N1; in Cpt treatment, C3 > C1 > C2 and N3 > N1 > N2; and in Etp treatment, C3 > C1 > C2 and N3 > N1 > N2. To confirm whether CHK1 cleavage is efficiently induced only by DNA damage-induced PCD, we further explored and then found that CHK1 cleavage efficiently occurs in LLnV- or LLnL-induced PCD (Fig. 1C). LLnV (also called MG115) and LLnL (also called MG101) are useful tools to examine the involvement of calpains, cathepsins, or proteasomes on an intracellular signaling pathway because both drugs are potent cell permeable inhibitors of calpains, cathepsins, or proteasomes [19]. Treatment with z-VAD-fmk also inhibited Etp, LLnV, or LLnL-induced CHK1 cleavage (Fig. 1C). As shown in Supplemental Fig. I, in HeLaS3 cells, all cleavages in Etp-induced PCD were inhibited by co-treatment with z-VAD-fmk. These results indicate that CHK1 cleavage occurs efficiently in DNA damage-induced PCD and certain types of protease inhibitor-induced PCD. Since it has been reported that PCD signals activate a certain type of serine protease such as HTRA2, AP24, and Cathepsin G [6,20–22], we examined the effects of some serine protease inhibitors, AEBSF, TLCK, or TPCK, on the CHK1 cleavage. As shown in Fig. 1D, all serine protease inhibitors we used inhibited the CHK1 cleavage induced by Etp treatment, however, PARP1 cleavage was slightly decreased. Consistent with this result, CASP3, CASP7, and CASP9 activation in ETP-treated cells was slightly inhibited by co-treatment with AEBSF (data not shown). These results suggest that serine protease family proteins are also involved in CHK1 cleavage in PCD. The most well-characterized serine protease is HTRA2, which enhances apoptotic cell death via interaction with the endogenous apoptosis inhibitor XIAP, so we analyzed the involvement of HTRA2 in CHK1 cleavage by using a knockdown method (Fig. 1E). HTRA2 knockdown by siRNA slightly reduced Etp-induced CHK1 cleavage. To further support the involvement of HTRA2 in CHK1 cleavage, we sought to analyze the effect on CHK1 cleavage using Ucf-101, which is the best-known inhibitor of HTRA2 [23]. As shown in Fig. 1F, chemical inhibition of HTRA2 completely inhibited CHK1 cleavage. These results show that HTRA2 is one of the candidate serine proteases involved in the regulation of CHK1 cleavage.

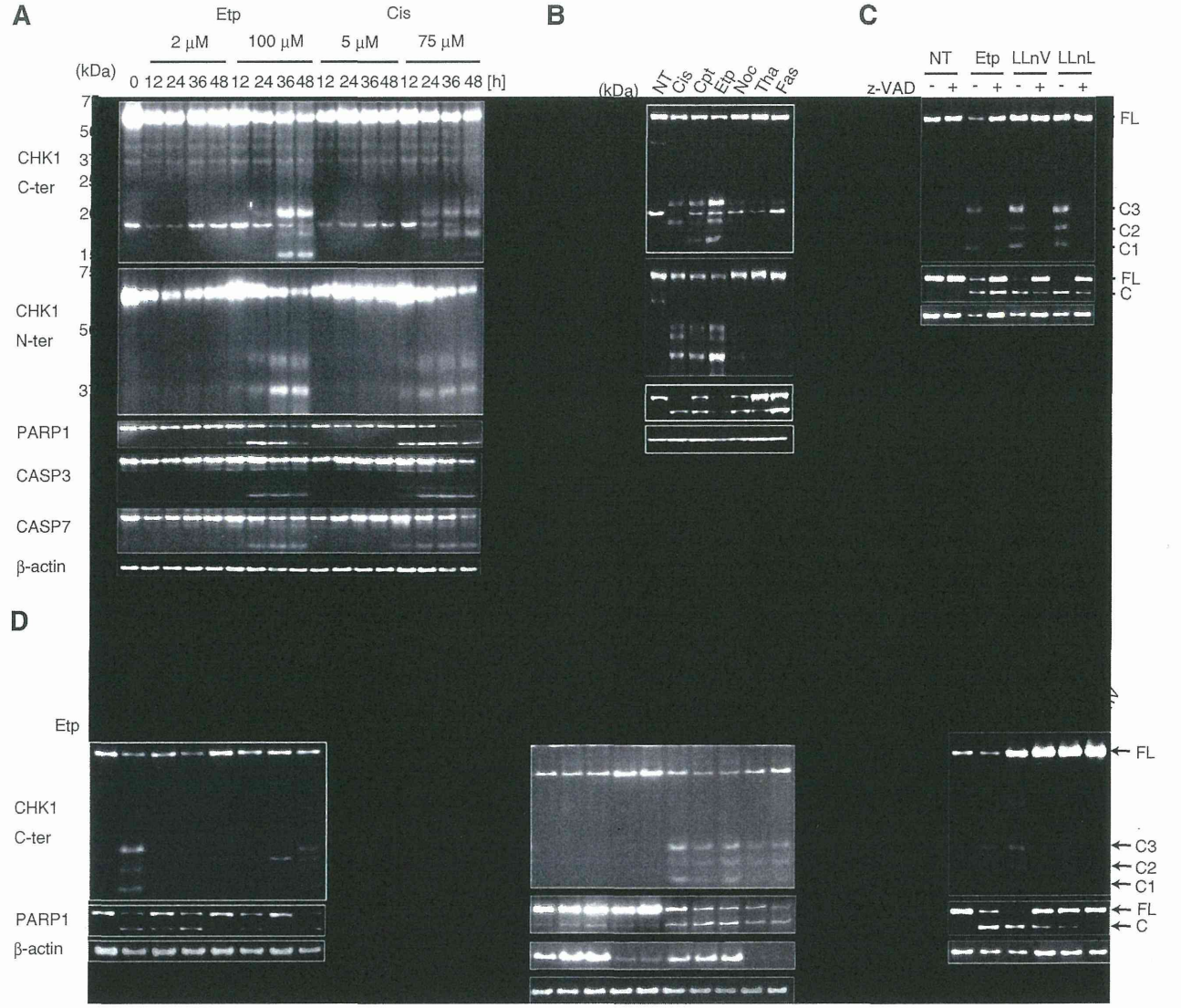

Fig. 1. Efficient CHK1 cleavage in DNA damage-induced PCD and the involvement of CASP and serine protease family. (A) U2OS cells were treated with the indicated doses of Etp or Cis for indicated times. The cell lysates were analyzed by Western blotting with the indicated antibodies. (B) U2OS cells treated with various apoptosis-inducing agents for 36 h were analyzed by Western blotting. NT, non-treatment; Cis, 60 μM Cis; Cpt, 20 μM Cpt; Etp, 100 μM Etp; Noc, 500 nM Noc; Tha, 2 μM Tha; FAS, 50 ng/mL anti-FAS (CH-11) and 20 μM Chx. (C) U2OS cells were pretreated in the absence or presence of 100 μM z-VAD-fmk for 1 h, and ETP, LLnV, or LLnL was then added into the medium at a final concentration of 100, 2, or 50 μM, respectively. After another 48-h incubation, the cells were harvested. The lysates were analyzed by Western blotting with the indicated antibodies. (D) U2OS cells were pretreated in the absence or presence of the indicated serine protease inhibitors (400 nM AEBSF, 300 nM TLCK, 80 nM TPCK) for 1 h, and ETP was then added into the medium at a final concentration of 100 μM. After another 48-h incubation, the cells were harvested. The lysates were analyzed by Western blotting with the indicated antibodies. The asterisk indicates a non-specific band. (E) siRNA transfected U2OS cells were treated with 100 μM ETP for 36 h. The lysates were analyzed by Western blotting with the indicated antibodies. Non-si: no siRNA, siScr: scramble siRNA, siHTRA2: HTRA2 siRNA. (F) U2OS cells were pretreated in the absence or presence of 50 μM Ucf-101 for 1 h, and ETP was then added into the medium at a final concentration of 100 μM. After another 48-h incubation, the cells were harvested. The lysates were analyzed by Western blotting with the indicated antibodies.

3.2. Identification of CASP family proteases responsible for CHK1 cleavage and the effect of cleavage on CHK1 kinase activity

As shown in Fig. 1, since all CHK1 cleavages in PCD were regulated in a CASP-dependent manner, we predicted that CASP family proteases directly catalyze CHK1 cleavage. Hence, we performed CHK1 cleavage assays using recombinant CASP2, CASP3, CASP6, CASP7, CASP8, CASP9, or CASP10, which are categorized as apoptotic CASPs [3–5]. Recombinant CHK1 was prepared as a protein fused with 3× FLAG tag at its N-terminus and 3× Myc tag at its C-terminus. The C-terminal products of CHK1 were detected by Western blotting using anti-Myc. The results showed that CHK1 is cleaved into two major products by CASP3 or CASP7 (Fig. 2A). Considering the molecular weights of cleavage products shown in Fig. 1, it was considered likely that the two major signals were from C3 (probably due to cleavage at D^{299}) and C1 (probably due to cleavage at D^{351}) fragments. A comparison to mobility of CHK1 cleavage fragments from the positive control (Etp-treated cell lysate expressing 3× FLAG-CHK1–3× Myc) supported this estimation (Supplemental Fig. II). To ensure that the two major products were from D^{299} and D^{351}, we examined whether a D299E or D351E mutation inhibits CASP3 or CASP7-mediated CHK1 cleavage. In D299E and D351E mutants, we detected only C3 and C1 fragments, respectively (Fig. 2B). This result demonstrates that C3 and C1 fragments are derived from cleavage at D^{299} and D^{351}, respectively. Furthermore, to aid prediction of the in vivo contribution of CASP3 and CASP7, we tested whether